Reducing Numerical Artifacts by Sacrificing Well-Balance for Rotating Shallow-Water Flow

Håvard Heitlo Holm[1] and Florian Beiser[1,2]

[1] SINTEF Digital, Mathematics and Cybernetics, Norway,
havard.heitlo.holm@sintef.no
[2] Norwegian University of Science and Technology,
Department of Mathematical Sciences, Norway

Abstract. We consider the problem of rotational shallow-water flow for which non-trivial rotating steady-state solutions are of great importance. In particular, we investigate a high-resolution central-upwind scheme that is well-balanced for a subset of these stationary solutions and show that the well-balanced design is the source of numerical artifacts when applied to more general problems. We propose an alternative flux evaluation that sacrifices the well-balanced property and demonstrate that this gives qualitatively better results for relevant test cases and real-world oceanographic simulations.

Keywords: high-resolution finite-volume schemes, rotating shallow-water equations, oceanography, numerical artifacts

1 Introduction

Over the past few years, we have developed a GPU-accelerated simulation framework [1] for oceanographic applications and ensemble prediction systems. At the core of the framework is a simplified ocean model based on the shallow-water equations in a rotational frame of reference. This hyperbolic system is solved using a slightly modified version of the numerical scheme proposed by Chertock et al. [2] (abbreviated as CDKLM). This is an explicit high-resolution finite-volume scheme that is conservative, second order, and consistent, formulated on Cartesian grids. Its main advantage compared to similar schemes is that it is well-balanced with respect to some non-trivial steady-state solutions in geostrophic balance, namely geostrophic jets along the coordinate axes. Hereby, the rotational pull on the jets is equal to the gravity-induced potential energy from a non-flat ocean surface. The geostrophic jets are however not the only steady-state solutions based on geostrophic balance, and in real-world oceanographic applications, rotational steady-states are often of greater importance.

The CDKLM scheme is based on central-upwind schemes [3], which are attractive as "black-box" solvers as they do not require solutions to the Riemann problem. An alternative to CDKLM is the earlier scheme proposed by Kurganov and Petrova [4] (abbreviated as KP), which also uses central-upwind flux evaluations but is not well-balanced for any non-trivial rotational steady-state solutions. When considering alternative numerical schemes, one that is well-balanced

Author accepted manuscript version of the publication by Håvard H. Holm & Florian Beiser. In Finite Volumes for Complex Applications X—Volume 2, Hyperbolic and Related Problems. 2023. Published version:
https://doi.org/10.1007/978-3-031-40860-1_19

for some geostrophic steady-state solutions and one that is not, it is easy to choose to implement the former also for more complex applications. However, as we will show in this paper, one should be more careful in this selection.

In this work, we demonstrate that the CDKLM scheme gives oscillatory artifacts and show that we can achieve solutions that are qualitatively better for rotational flow by using a non-well-balanced variation of CDKLM. Thereafter, we continue by investigating how to tune the resulting finite-volume scheme when applied to real-world oceanographic problems.

2 Rotational Shallow Water Equations

The shallow water equations in a rotational frame of reference are given by

$$\begin{bmatrix} \eta \\ hu \\ hv \end{bmatrix}_t + \begin{bmatrix} hu \\ hu^2 + \frac{1}{2}gh^2 \\ huv \end{bmatrix}_x + \begin{bmatrix} hv \\ huv \\ hv^2 + \frac{1}{2}gh^2 \end{bmatrix}_y = \begin{bmatrix} 0 \\ fhv \\ -fhu \end{bmatrix} + \begin{bmatrix} 0 \\ ghH_x \\ ghH_y \end{bmatrix} \tag{1}$$

and conserve mass and momentum. The variable η represents the water surface as a deviation from the mean equilibrium depth H, so that $h = H + \eta$ becomes the total water depth. Momentum is given by hu and hv in x- and y-direction, respectively. Furthermore, g is the gravitational constant, and f is the Coriolis parameter, which is a function of latitude. We define the vector $\mathbf{q} = [\eta, hu, hv]^T$ to contain the conserved variables, so that we can write (1) as

$$\mathbf{q}_t + \boldsymbol{\mathcal{F}}(\mathbf{q})_x + \boldsymbol{\mathcal{G}}(\mathbf{q})_y = \mathbf{S}(\mathbf{q}) \, . \tag{2}$$

Rotating steady-states solutions of (1) are given by geostrophic balances, where

$$u_x + v_y = 0 \, , \qquad g\eta_x = fv \, , \quad \text{and} \quad g\eta_y = -fu \, . \tag{3}$$

In [2], the last two expressions are rewritten in terms of potential energies as

$$K(x,y) := g\left(\eta - \int_{-\infty}^{x} \frac{f}{g} v \, \mathrm{d}x'\right), \qquad L(x,y) := g\left(\eta - \int_{-\infty}^{y} \frac{f}{g} u \, \mathrm{d}y'\right), \tag{4}$$

so that they can be written as $K_x = 0$ and $L_y = 0$. In particular, the CDKLM scheme is well-balanced with respect to the geostrophic jets

$$u \equiv 0, \quad v_y \equiv 0, \quad \eta_y \equiv 0, \quad H_y \equiv 0, \quad K \equiv \text{const}, \tag{5}$$

$$v \equiv 0, \quad u_x \equiv 0, \quad \eta_x \equiv 0, \quad H_x \equiv 0, \quad L \equiv \text{const}, \tag{6}$$

which are special cases of (3).

3 Finite Volume Schemes

In the following, we summarize only the relevant parts of the CDKLM scheme; the reader can find all details in [2]. We start by discretizing the domain in a

regular Cartesian grid with cells of size $(\Delta x, \Delta y)$, and define $\mathbf{Q}_{j,k}$ to be the average of $\mathbf{q}$ within the cell with center at $\left((j+\frac{1}{2})\Delta x,\ (k+\frac{1}{2})\Delta y\right)$. Equation (2) can then be written in semi-discrete form as

$$\frac{\partial \mathbf{Q}_{j,k}}{\partial t} = -\frac{\mathbf{F}_{j+1/2,k} - \mathbf{F}_{j-1/2,k}}{\Delta x} - \frac{\mathbf{G}_{j,k+1/2} - \mathbf{G}_{j,k-1/2}}{\Delta y} + \mathbf{S}(\mathbf{Q}_{j,k}). \tag{7}$$

The system is solved in time with the second-order total-variation-diminishing Runge-Kutta scheme [5] with time steps satisfying the CFL condition. In the rest of the paper, we focus on the spatial reconstruction and fluxes.

3.1 Well-balanced scheme

To design a well-balanced finite-volume scheme for (1) with respect to (5) and (6), Chertock et al. [2] propose to reconstruct the face values of $\mathbf{q}$ by computing the slopes of the equilibrium variables $\mathbf{p} = [u, v, K, L]^T$ rather than the slopes of $\mathbf{q}$ directly. Values for $K_{j,k}$ and $L_{j,k}$ are obtained by evaluating the integrals in (4) by a recursive sum starting from zero at the boundary. Note that the recursive sums for K and L mostly cancel in the reconstruction and are reduced to local operations [1, Sect. 3.1]. The slopes are then found by the generalized minmod limiter (c.f. [6]), which in the x-direction is

$$(\mathbf{p}_x)_{j,k} = \text{minmod}\left(\theta\frac{\mathbf{p}_{j+1,k} - \mathbf{p}_{j,k}}{\Delta x}, \frac{\mathbf{p}_{j+1,k} - \mathbf{p}_{j-1,k}}{2\Delta x}, \theta\frac{\mathbf{p}_{j,k} - \mathbf{p}_{j-1,k}}{\Delta x}\right), \tag{8}$$

where $\theta \in [1, 2]$ controls numerical dissipation.

Using $(\mathbf{p}_x)_{j,k}$ and $(\mathbf{p}_x)_{j+1,k}$, we can reconstruct one-sided point values for $\mathbf{q}$ at the face between the two cells as $\mathbf{Q}^r_{j+1/2,k}$ and $\mathbf{Q}^l_{j+1/2,k}$ from the right and left, respectively, using the discretized version of (4) to reconstruct values for η. The flux terms in (7) are computed using the central-upwind (CU) scheme [3]

$$\mathbf{F}^{(i)}_{j+1/2,k} = \frac{a^+\boldsymbol{\mathcal{F}}\left(\mathbf{Q}^l\right) - a^-\boldsymbol{\mathcal{F}}\left(\mathbf{Q}^r\right)}{a^+ - a^-} + \frac{a^+a^-}{a^+ - a^-}\left(\mathbf{Q}^r - \mathbf{Q}^l\right) \tag{9}$$

for $i = 1, 2$, where we have omitted the subscript $(\cdot)_{j+1/2,k}$ for all $\mathbf{Q}$ (including its entries) and a variables for readability. The variables a^+ and a^- represent the largest positive and negative wave speeds at the cell interface, respectively,

$$a^\pm = \begin{matrix}\max\\ \min\end{matrix}\left\{u^l \pm \sqrt{gh^l},\quad u^r \pm \sqrt{gh^r},\quad 0\right\}. \tag{10}$$

For the scheme to be well-balanced with respect to (6), however, Chertock et al. [2] propose to use a standard-upwind (SU) scheme for $\mathbf{F}^{(3)}_{j+1/2,k}$, given by

$$\mathbf{F}^{(3)}_{j+1/2,k} = \begin{cases} h^r u^r v^r, & \text{if } u^r + u^l > 0,\\ h^l u^l v^l, & \text{otherwise.}\end{cases} \tag{11}$$

The scheme is defined analogously in the y-direction, where the CU flux in (9) is used for $\mathbf{G}^{(i)}_{j,k+1/2}$, $i = 1, 3$, and the SU in (11) is used for $\mathbf{G}^{(2)}_{j,k+1/2}$.

3.2 Unbalanced alternatives

As we will see in Section 4, the use of the SU flux in (11) produces artifacts when applying CDKLM to rotational and realistic problems. To investigate the problem, we consider a convex combination of the two fluxes

$$\mathbf{F}^{(3)}_{j+1/2,k} = \phi(\mathbf{F}_{SU})^{(3)}_{j+1/2,k} + (1-\phi)(\mathbf{F}_{CU})^{(3)}_{j+1/2,k}, \tag{12}$$

in which $\mathbf{F}_{CU}$ comes from (9), $\mathbf{F}_{SU}$ comes from (11), and $\phi \in [0,1]$.

In contrast to CDKLM, KP reconstructs the slopes of $\mathbf{q}$ using the conserved variables directly and evaluates all flux components using the central-upwind scheme. We implement (12) also for KP and compare it with CDKLM to better assess the effects of different reconstructions and flux terms in isolation.

4 Numerical Experiments

We consider five experiments to evaluate the pros and cons of using the reconstruction and flux that make the scheme well-balanced for geostrophic jets.

Case A: Radial wave without rotation. First, we consider a simple radial wave in a non-rotating domain (meaning $f = 0$), initialized by

$$\eta(x,y,0) = \exp^{-10^{-5}(x^2+y^2)}, \quad \text{and} \quad hu(x,y,0) = hv(x,y,0) = 0. \tag{13}$$

The domain consists of 400×400 cells with $\Delta x = \Delta y = 100\,\mathrm{m}$, centered at the origin. The equilibrium depth is $H(x,y) = 60\,\mathrm{m}$.

Figure 1 shows hv at $t = 1000\,\mathrm{s}$ in the central part of the domain after most of the energy has traveled outwards. In the plots of the y-momentum shown in the two leftmost plots for the CDKLM scheme with SU and CU fluxes, we clearly see an oscillating artifact when using SU. This is even more pronounced in the right-hand plot of Fig. 1, which shows a cross section at $y = -1\,\mathrm{km}$. The CU flux gives numerical artifacts along the grid diagonals, but these are smooth in contrast to the SU artifacts. Both solutions are symmetric in hv and hu, and the artifacts are observed for any spatiotemporal resolution satisfying the CFL conditions with Courant number less or equal to 0.5.

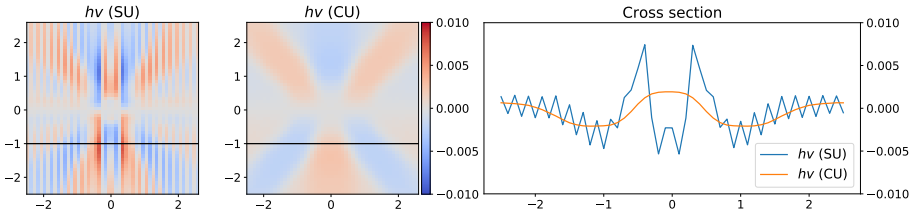

Fig. 1. Artifacts in hv from an initial bump using CDKLM with SU flux (left) and CU flux (center), and cross section of hv at $y = -1\,\mathrm{km}$ (right).

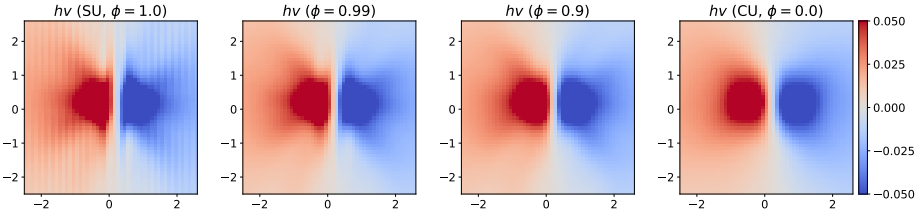

Fig. 2. Numerical steady-states in hv from an initial bump with different ϕ-values in flux (12) in the presence of Coriolis forces.

Note that with $f = 0$, the CDKLM reconstruction reduces to that of the the KP scheme. We have implemented the KP scheme independently, and get exactly the same results as for CDKLM using both types of fluxes. This excludes the possibility that the artifacts are caused by a programming bug.

Case B: Rossby adjustment. We continue by considering Rossby adjustment, in which a rotational steady state is generated when running Case A with $f = 0.0012\,\mathrm{s}^{-1}$. The presence of Coriolis forces will establish a rotating bump in the center of the domain and create a steady-state that is not covered by the jets described in (5) and (6).

In Fig. 2, we consider the flux in (12) and assess different values for ϕ. The leftmost plot uses $\phi = 1.0$, which corresponds to a pure SU flux as in the original CDKLM scheme, whereas $\phi = 0.0$ to the far right corresponds to the CU flux. Again, hu and hv are symmetric, so we only show results for hv. We see a similar nonphysical oscillation pattern as in Case A when using the SU flux, and the rotating bump is dragged along the grid axes. In contrast, the CU flux results in a circular bump that captures (3) much better. It is interesting that it is sufficient to introduce just a small CU contribution to the SU flux to improve the numerical behavior, and the results are already significantly better with $\phi = 0.9$. The figures are visually the same when using KP.

Case C: Kelvin wave. Kelvin waves are relatively fast travelling waves trapped along the coast by the Coriolis forces. They are travelling with the coast to their right on the Northern hemisphere and are important in realistic applications, as the tides often form them. Here, we consider a periodic domain in the east-west direction with wall boundary conditions in the north and south, and initialize a wave travelling eastwards along the southern wall. Sufficiently small waves follow linear physics and give periodic solutions, but the amplitudes used herein give nonlinear responses that develop a shock over time; see [7, Sect. 4.4] for details.

Figure 3 compares the CDKLM and KP schemes when using the CU flux and $\theta = 1.5$ for both, meaning that the only difference is in the slope reconstruction. The figure shows the solution after ten periods, corresponding to more than 60,000 time steps, at two cross sections for fixed y. We see how both schemes capture the nonlinear behavior of large waves. CDKLM manages, however, to

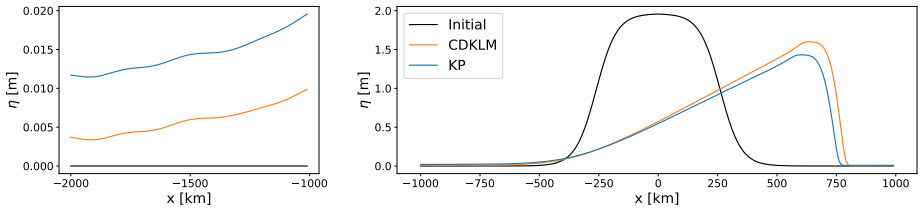

Fig. 3. Cross-sectional plots of a Kelvin wave after ten periods for CDKLM and KP with CU flux and $\theta = 1.5$. Tail on the left and wave center on the right panel.

maintain a taller wave front than KP, whereas KP produces a long nonzero tail. We argue that these results favor CDKLM for this case.

Case D: Geostrophic jets. We consider a double geostrophic jet that satisfies the steady-state given by (6), with one jet travelling eastward in the northern part of the domain and an westward jet in the southern part. We use periodic boundary conditions; the case is described in full in [8, Sect. 5]. This case exposes what we lose by not using the well-balanced SU flux for CDKLM, as this flux preserves this steady state for any slope limiter θ.

Figure 4 shows a cross section along y after running CDKLM for a long time using the CU flux with different values for θ. With $\theta = 1.0$, the numerical dispersion smooths out the jet streams significantly, but a moderate increase in θ compensates for using a non-balanced flux, and the jets stay captured and only cap the extrema slightly. With the maximal possible $\theta = 2.0$, we lose only 4.5% of the momentum in the center of the jets.

To see how much of the CU flux we can incorporate without diminishing the preservation of geostrophic jets, we run the experiment for decreasing values of ϕ with fixed $\theta = 1.8$. For all $\phi \geq 0.52$, we conserve the maximum momentum within 4.5%.

Case E: Real-world simulation. Finally, we study the consequence of using different flux terms and slope limiters when using the CDKLM scheme for

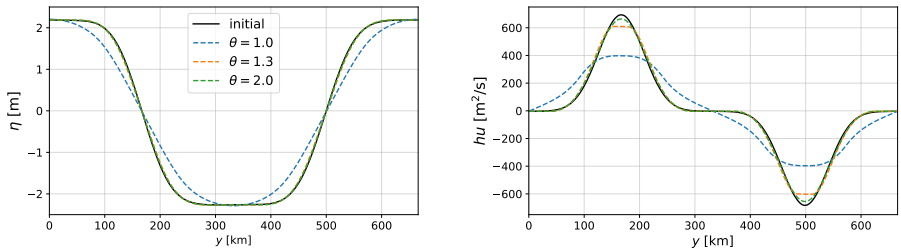

Fig. 4. A double jet state after 9 simulation days with the CU flux: the plots show cross-sections of η (left) and hu (right).

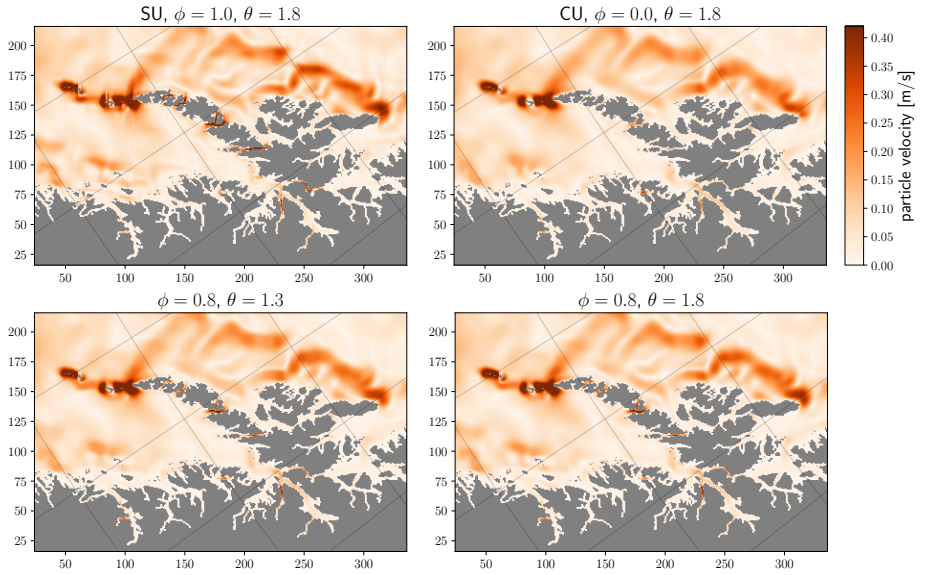

Fig. 5. Real-world simulation for the Lofoten archipelago in Northern Norway. The axes show position within the computational domain in km.

simulating a real-world oceanographic scenario. Here, we utilize the full GPU-accelerated framework from [1], in which land mask, bathymetry, initial and boundary conditions, domain orientation, and wind forcing are taken from the operational model NorKyst800 [9], with 800 m horizontal resolution.

Figure 5 shows water velocity at 23 h for a few selected values of ϕ and θ for CDKLM. The first thing to notice is how the SU flux gives visible artifacts around the outermost islands at $(100, 150)$. Secondly, the CU scheme gives visibly slower currents than SU, e.g., at $(300, 150)$. Since the tidal Kelvin wave follows the coast from left towards right, the Lofoten islands trap the tidal wave, causing strong currents in between the islands. With CU, we do not resolve this, but setting $\phi = 0.8$ helps significantly. It is hard to see visual differences between setting $\theta = 1.3$ and $\theta = 1.8$, but examining cross sections (not shown) reveals that we indeed get sharper fronts but no oscillations with the latter, which is preferred.

5 Conclusion

We have demonstrated numerical artifacts in the CDKLM scheme in cases that differ from geostrophic balanced jets along the coordinate axes. We identified the source of the oscillations to be the standard-upwind flux in the *huv* fluxes. By combining the standard-upwind flux with the central-upwind flux with a factor ϕ, we reduced unintended numerical behavior significantly and made the results more physical, even though we lose the well-balanced property for the jets.

We have illustrated the artifacts in Cases A and B, where Case B indicates that combining the SU flux with a small factor of CU is sufficient to smooth out these oscillations. In Case C, we see that the slope reconstruction in CDKLM still gives a small advantage over the more standard reconstruction used by the KP scheme. By using a large value θ in the slope limiter, we demonstrated that also pure CU can preserve the geostrophic jets from Case D within acceptable tolerances. Case E, however, shows that the pure CU flux is unable to capture strong realistic currents in narrow straits. The conclusion is then to use values close to $\phi = 0.8$ and $\theta = 1.8$ as flux parameter and slope limiter, respectively, for real-world oceanographic applications. This reduces the observed artifacts and gives a practical compromise between the well-balanced SU flux and the smoother behaving CU flux.

Acknowledgement This work is supported by the Research Council of Norway (RCN) through grant number 310515 (Havvarsel). The numerical examples are made with the GPU Ocean software [10], and can be reproduced by [11].

References

1. A. Brodtkorb and H. Holm. Coastal ocean forecasting on the GPU using a two-dimensional finite-volume scheme. *Tellus A*, 73(1):1–22, 2021.
2. A. Chertock, M. Dudzinski, A. Kurganov, and M. Lukácová-Medvidová. Well-balanced schemes for the shallow water equations with Coriolis forces. *Numer. Math.*, 138(4):939–973, 2017.
3. A. Kurganov, S. Noelle, and G. Petrova. Semidiscrete central-upwind schemes for hyperbolic conservation laws and Hamilton-Jacobi equations. *SIAM J Sci Comput*, 23(3):707–740, 2001.
4. A. Kurganov and G. Petrova. A second-order well-balanced positivity preserving central-upwind scheme for the Saint-Venant system. *Commun Math Sci*, 5(1):133–160, 03 2007.
5. S. Gottlieb and C.-W. Shu. Total variation diminishing Runge-Kutta schemes. *Math. Comput.*, 67(221):73–85, 1998.
6. K.-A. Lie and S. Noelle. On the artificial compression method for second-order nonoscillatory central difference schemes for systems of conservation laws. *SIAM J Sci Comput*, 24(4):1157–1174, 2003.
7. H. Holm, A. Brodtkorb, G. Broström, K. Christensen, and M. Sætra. Evaluation of selected finite-difference and finite-volume approaches to rotational shallow-water flow. *Commun Comput Phys*, 27(4):1234–1274, 2020.
8. H. Holm, M. Sætra, and P. van Leeuwen. Massively parallel implicit equal-weights particle filter for ocean drift trajectory forecasting. *J. Comput. Phys.: X*, 6(0314):100053, 2020.
9. J. Albretsen, A. Sperrevik, A. Staalstrøm, A. Sandvik, and F. Vikebø. NorKyst-800 report no. 1: User manual and technical descriptions. Technical Report 2, Fisken og Havet, Institute of Marine Research, 2011.
10. A. Brodtkorb, H. Holm, M. Sætra, and F. Beiser. GPU Ocean, 2023. DOI: 10.5281/zenodo.7938844.
11. H. Holm and F. Beiser. Supplementary material for "Reducing numerical artifacts by sacrificing well-balance for rotating shallow-water flow", 2023. DOI: 10.5281/zenodo.7938887.